RESEARCH ARTICLE

VOLCANICA

Catastrophic lava flow levee failure: precursors, processes, and implications

Elisabeth Gallant [*α, β], Hannah R. Dietterich[γ], Matthew R. Patrick[β], David Hyman[δ], Brett B. Carr[ε], John Lyons[γ], and Elinor S. Meredith[ζ]

[α]University of Hawai'i, Department of Geology, Hilo, HI, 96720, USA.
[β] U.S. Geological Survey, Hawaiian Volcano Observatory, Hilo, HI, 96720, USA.
[γ] U.S. Geological Survey Alaska Volcano Observatory, Anchorage, AK, 99508, USA.
[δ] U.S. Geological Survey, Advanced Research Computing, Lakewood, CO, 80225, USA.
[ε] University of Arizona, Lunar and Planetary Laboratory, Tuscon, AZ, 85721, USA.
[ζ] Faculty of Geo-Information Science and Earth Observation (ITC), University of Twente, Enschede, The Netherlands.

Abstract

During an effusive eruption crisis the initial advance of a lava flow is typically the primary focus of model forecasts and hazard management efforts. Flow branching and lateral expansion of lava flows can pose significant dangers within evolving flow fields throughout the duration of an eruption and are an underappreciated hazard. We use field monitoring, infrasound, time lapse imagery, and LiDAR data collected during the 2018 lower East Rift Zone eruption of Kīlauea (Hawai'i, USA) to track the origins, progression, and implications of a flow branching event caused by catastrophic levee failure. Our analyses show that surges in effusion rate, rheologic transitions in the channel, slope-breaks, pre-existing topographic highs, and the structure of perched levee walls all played a role in the failure of the levee and subsequent re-routing of the lava flow. Failure of perched lava structures leads to an acutely hazardous situation because lava impounded by the structure can rapidly inundate the landscape. This is the first time a levee failure event has been observed in such detail with numerous monitoring techniques; this unprecedented level of observation provides quantifiable insights into levee failure processes that have important implications for hazard mitigation and an improved understanding of lava flow emplacement dynamics.

Keywords: Volcanic Hazards; Effusive eruption; Kilauea.

Submitted: 2024-04-24 | Accepted: 2024-11-04 | Published: 2025-01-31

Editor: O. Chevrel | Typesetter: J. Farquharson

1 Introduction

Lava flows are dynamic hazards that can evolve rapidly and have a devastating impact on the populations they intersect with. Flows that branch and deviate from initial routes as eruptions progress are particularly problematic because they can inundate areas previously considered to be at lower risk with little warning and impact evacuation routes, emergency services, and cut off access to infrastructure. The 1669 eruption of Etna (Italy) branched and diverted numerous times and destroyed or partially inundated seven towns, including Catania, within a month of the eruption's onset [Branca et al. 2013]. Later breakout flows to the north and southwest during the 2014–2015 eruption of Fogo, Cabo Verde, had a devastating impact on buildings and infrastructure [Jenkins et al. 2017]. The 2021 lava flow on La Palma (Spain) contained numerous branches that destroyed 1345 homes [Pankhurst et al. 2022]. These examples represent a small fraction of effusive eruptions with complex emplacement histories into populated areas.

Flow branching events can be categorized as primary or secondary in origin. Primary flow branching events are those that occur as the flow is advancing and bifurcates due to interactions with pre-existing topography, whereas secondary events occur due to levee failure or oveurflowing of the flow's own existing lava structures. The controls, precursors, and implications of these secondary flow branching events are not well understood, with evidence for fluctuating lava supply rate [Tarquini and de'Michieli Vitturi 2014; Rader et al. 2017; Patrick et al. 2019; Peters et al. 2022], channel blockages [Guest et al. 1987; Lipman and Banks 1987], and levee weakness [Guest et al. 1987; Orr et al. 2022] all playing a role. Rapid release of ponded lava during a secondary branching event can generate acutely hazardous flow lobes due to high flow velocities induced by dam-break dynamics [Patrick and Orr 2012; Belousov and Belousova 2018; Burgi et al. 2020]. Such events have been observed at numerous volcanoes, though not with the temporal resolution of potential controls and their effects to track their origins and evolution from start to finish [Applegarth et al. 2010; Favalli et al. 2010; Orr et al. 2022].

Operational hazard assessment for volcanic eruptions relies on a combination of geophysical monitoring data, field observations, and forecast modeling. In an effusive eruption, observatories must rapidly assess and communicate areas at risk throughout an eruptive crisis, from initial warning and early detection of vent locations to the evolution of lava flow fields [Del Negro et al. 2013; Harris et al. 2017; Neal et al. 2019]. For lava flow hazard assessment, the initial advance of a flow has been the primary focus of monitoring and crisis response, because it dictates where and how quickly the first areas downslope will be impacted [Chevrel et al. 2022]. When a new flow is advancing, the vent location or flow front is often used to initiate or update forecasts of where lava will next inundate. Over time, this approach treats the vent and established lava flow field as static and may preclude "upstream" processes from influencing the inundation path.

*egallant@hawaii.edu

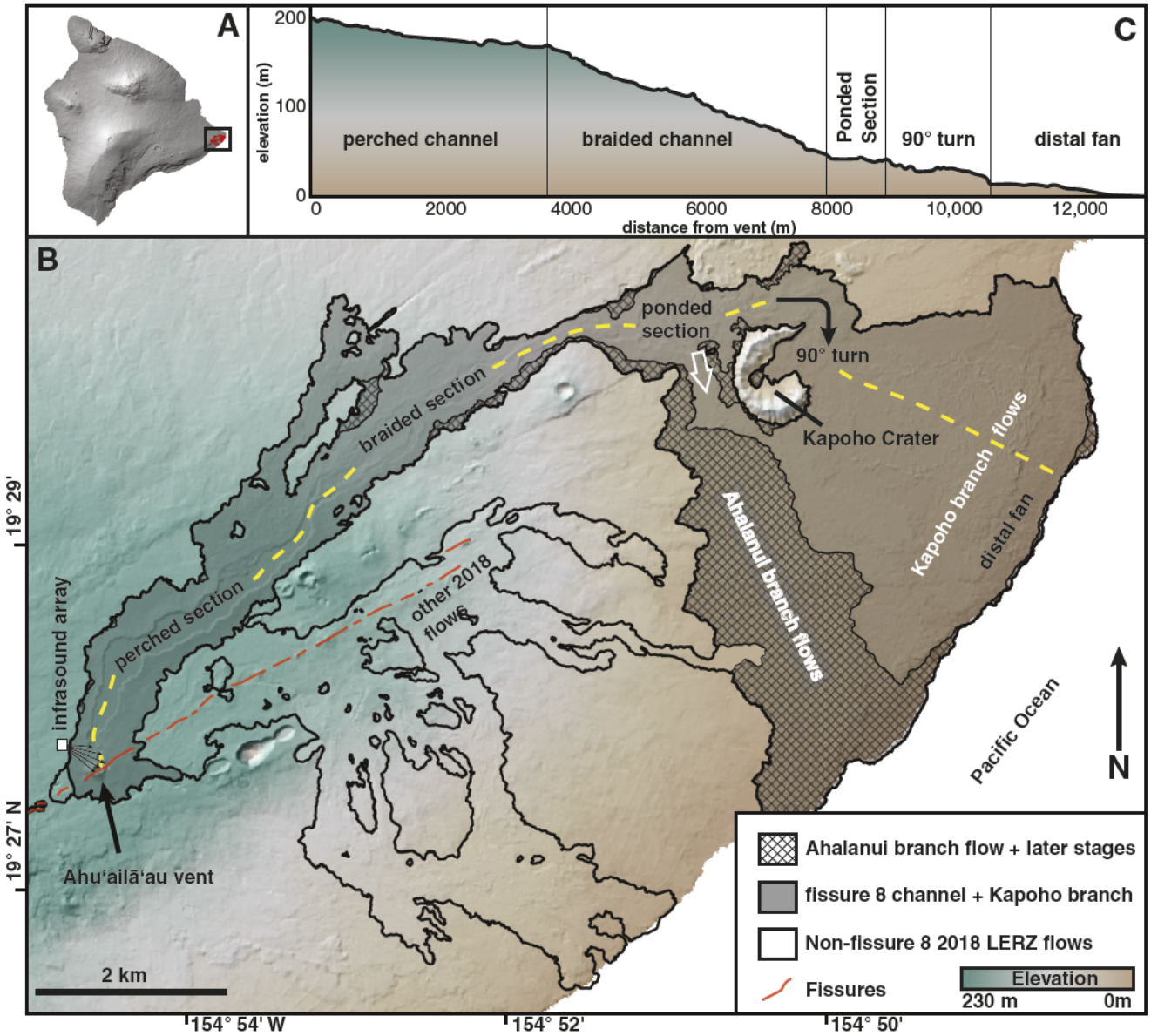

Figure 1: Area map and elevation profile of the fissure 8 flow with important features notated. [A] Inset image showing the location of the study area. [B] Map of the 2018 lower East Rift Zone eruption features. The fissure 8 flows are shown, broken out into the early channel growth and Kapoho branch (gray shading) and later stage flows and Ahalanui branch (cross-hatched). We focus our reconstruction of events on data and observations from the Ahalanui branch (whose initiation point is indicated by the open white arrow), the ponded section, and the 90° turn. Non-fissure 8 flows issued during the 2018 eruption are outlined. [C] Elevation profile showing slope differences along the length of the flow from the vent to the ocean entry, noted in B as the yellow dashed line.

We investigate a secondary flow branching event that was documented in unprecedented detail during the 2018 lower East Rift Zone eruption of Kīlauea, Hawaiʻi (USA), to better understand the processes that lead to secondary branching and subsequent acute lateral hazards (Figure 1). This newly formed flow branch, which we informally call the Ahalanui branch, caused a catastrophic rerouting of a long-lived fissure 8 lava channel and destroyed 86 built structures and 5.7 km^2 in land. The Ahalanui branch occurred halfway through the eruption and took approximately one day to unfold. The evolution of this event was captured by LiDAR surveys, thermal and standard optical imagery, geophysical monitoring, uncrewed aircraft system (UAS) videos, and field observations through time, allowing detailed investigation of the precursors, dynamics, and impacts of the event on a timescale of hours to minutes, as opposed to days.

2 Background

2.1 Flow branching

Primary branching of ʻaʻā lava flows is controlled by the supplied volume and interactions between the flow front and the local topography during flow advance [Dietterich and Cashman 2014]. Secondary branches from lava overflows and

breakouts, conversely, are cooling limited behaviors that often occur when relatively stable effusion rates oscillate [Patrick et al. 2019]. A rapid change in lava viscosity, an order of magnitude greater over short distances [Sehlke et al. 2014], occurs as a function of both heat loss, crystallization, and flow instabilities [Di Fiore et al. 2021; Culha et al. 2023] and can act as an internal dam. This can then become a source of branching if the effusion rate rises and lower viscosity lava backs up against this more stagnant lava and overflows or breaks out of a channel [Patrick et al. 2019]. Changes in viscosity that influence surface morphology, crust development, and the location where open flow within the channel ends [Cashman et al. 1999; Hon et al. 2003]. While is possible that end of the open channel might also correspond to the pāhoehoe–ʻaʻā transition [e.g. Sehlke et al. 2014], we here focus on the open channel's extent and thus use the phrase "transitional channel zone" to describe the zone between destabilized channel and the dispersed flow as defined by Lipman and Banks [1987].

The drivers of these secondary branching events and controls on their location, timing, and impacts have been observed at Etna, Holuhraun (Iceland), and Mauna Loa and Kīlauea (USA), but have not been well quantified [Lockwood et al. 1985; Guest et al. 1987; Applegarth et al. 2010; Favalli et al. 2010; Dietterich and Cashman 2014; Pedersen et al. 2017; Lormand et al. 2020]. The mechanics of breakouts caused by catastrophic levee failures are particularly understudied, as only a few of these events have been witnessed and documented [Lormand et al. 2020; Orr et al. 2022].

2.2 Levee failure

Levee failures can occur when an overflow thermomechanically erodes a levee (top-down) or when lava intrudes into a levee and structurally undermines it (bottom-up). Top-down failure modes have been observed during the Maunaulu eruption of Kīlauea (1969–1974) and the 1976, 1981, and 1983 eruptions of Etna [Guest et al. 1987; Harris et al. 2017; Lormand et al. 2020]. These failures are caused by fluctuations in effusion rate, which lead to changes in flux through the channel that, in turn, cause overhanging portions of the levee walls to fail and fall into the channel and lead to blockages downstream and eventual levee breach. The levee failure that led to the Monte Grosso flow, emplaced during the 2001 eruption of Etna, was likely due to the transient increase in effusion [Applegarth et al. 2010; Favalli et al. 2010]. Two major blockage-induced overflows re-routed portions of the 1984 Mauna Loa eruption 15 km down-channel from the source vent, eroding the levee underneath the overflow [Lockwood et al. 1985; Dietterich and Cashman 2014]. Levee failures of several small shields in 2007–2008 during the Puʻuʻōʻō eruption of Kīlauea were driven by "seeps" of viscous spiny lava, which had extruded from the shield levees prior to collapse [Patrick and Orr 2012]. Density-driven seeps also played a role in failure of a rootless shield that had been inactive for a month and its subsequent lava flow in 2014 [Orr et al. 2022]. The potential for stagnant perched features to fail in this way extends the duration of the local lava flow hazard potential from structures that store and insulate lava.

2.3 2018 lower East Rift Zone eruption and fissure 8 activity

Eruptive activity along Kīlauea's lower East Rift Zone began on May 3rd, 2018, in the Leilani Estates neighborhood [Neal et al. 2019] (Figure 1). A total of 24 fissures opened over a 6.8 km-long segment of the rift in the first three weeks of the eruption [Gansecki et al. 2019; Neal et al. 2019]. The second phase of the eruption saw the re-activation of several fissures and the emplacement of lava flows that eventually reached the coast [Gansecki et al. 2019; Meredith et al. 2022]. The third and most destructive phase of the eruption began on May 28th, 2018, at the re-activated fissure 8 (the cone that formed over the next several weeks would eventually be known as Ahuʻailāʻau). The eruption ended on September 5th, 2018, after four months of activity. The ~1.2 km^3 of lava erupted over this period buried 32 km^2 of land, impacted 1929 structures (damaged or destroyed), and caused US$800 million worth of damage [Meredith et al. 2022].

The main fissure 8 channel system was established between May 28th and June 3rd, 2018, during advance of the ʻaʻā flow to the ocean, and was continuously supplied through early August 2018. This supply was accompanied by fluctuations in effusion rate, which helped build a perched pāhoehoe channel system. Major components of the fissure 8 system include the vent and spillway, a perched channel proximal to the vent, a braided channel, a ponded section, a narrow section that takes a 90° turn around the cone at Kapoho Crater, and a distal fan that fed the ocean entry (Figure 1).

The flow sourced from the reactivated fissure 8 reached 13.5 km in 6 days as it advanced to the coast. The initial channel route, informally called the Kapoho branch, went along the north side of Kapoho Crater, before turning sharply to the south along the eastern side of the cone (~90° bend), and finally eastward into Kapoho Bay. A small lobe broke out and encircled the cone on June 4th, 2018—this short-lived feature would be exploited by the Ahalanui branch mid-way through the eruption. The main flow fed an ocean entry at Kapoho Bay and widened the footprint of the distal portion of the flow field during most of June 2018. This distal fan remained relatively stable until the end of June, when the previously open channel into the ocean began to stagnate, crust over, and retreat from the ocean entry area (Figure 2). Flow through the fan still fed the ocean entry at this time. The active channel continued to retreat up through the distal fan section through early July. A branching event on July 9th produced a new flow lobe that initially claimed 40 structures and entered the ocean at Ahalanui Beach Park on July 11th. It continued to build up a broad ʻaʻā delta until effusion waned in early August. The final phase of activity was a lava pond that resided in Ahuʻailāʻau until September 5th, 2018. GIS data that document chronological lava advance and flow field growth are provided in Zoeller et al. [2019]. Our analysis focuses on the branching event that occurred on July 9th, 2018, which formed the Ahalanui branch.

During this fissure 8-dominated phase of the eruption, near-daily caldera collapse events at the summit of Kīlauea caused the piston block drops that pressurized the magmatic system each time and generated surges in effusion rate 40 km down-rift at the Ahuʻailāʻau vent within minutes via pressure wave propagation. Bulk effusion rates would more than dou-

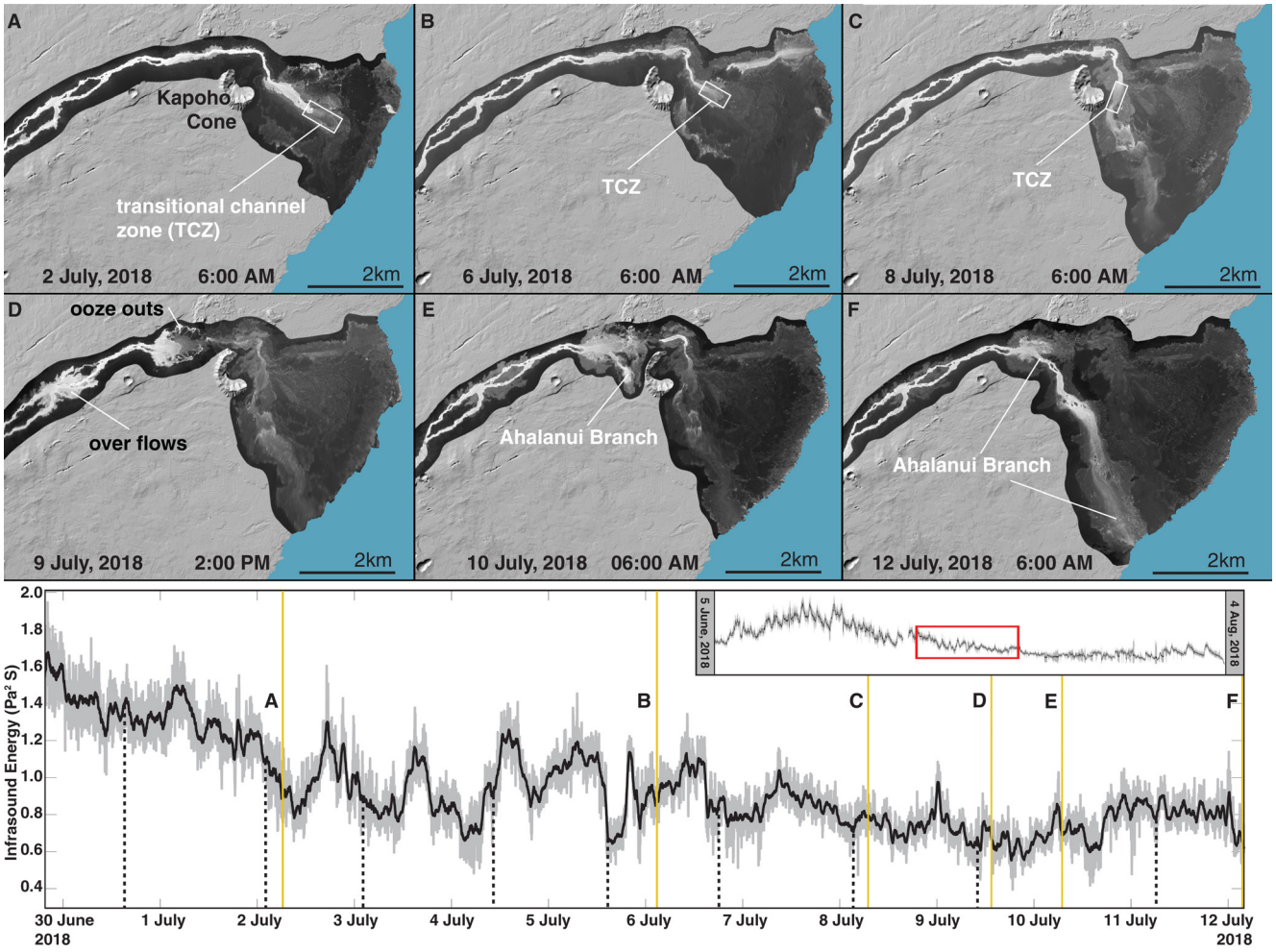

Figure 2: The progression of the branching event shown through thermal maps and infrasound energy from July 2nd [A] through July 12th [F] is shown in the upper panels. The thermal images highlight the progressive up-channel movement of the transitional channel zone in the week prior to the branching event, the syn-event expansion of the ponded area via ooze-outs, and the establishment of the Ahalanui branch. The thermal images have been cropped around the footprint of the flows and indicate relative temperatures from hot (white) to cold/ambient temperature (black), with gray indicating portions of the flow that are less active but still above ambient temperature. The lower panel inset shows the infrasound data (the oscillation of energy at the vent) that was collected during the eruption and the main section highlights the period of time leading up to and shortly after the branching event in greater detail (also noted by the red box). The yellow lines identify when each of the thermal images were captured to provide additional context. Caldera collapse events are noted by the dashed black lines.

ble their pre-surge levels within two hours of onset (548 to 1400–1700 $m^3\ s^{-1}$), and would then decay over the next day or two [Patrick et al. 2019; Dietterich et al. 2021]. The surge of new lava at the vent then propagated down the open channel, traversing 8 km in approximately 13 hours. The propagating surge temporarily increased the flow velocity and depth in the channel, generating progressive overflows as the lava stage rose and overtopped the levees as the surge propagated [Patrick et al. 2019].

3 Data and Methods

The various data used in this analysis were collected by the U.S. Geological Hawaiian Volcano Observatory and their affiliates during the 2018 eruption. An aerial LiDAR survey was flown in several passes from July 8th through 12th, 2018. The full associated data set has a point density of 18–100 points/m^2 and was post-processed to 0.5-m resolution bare-earth digital elevation models (DEMs). We isolated the data collected before and after the branching event by date to produce DEMs from July 8th and 10th, 2018 (based on local time). The original dataset and its metadata are available for download from OpenTopography and the DEMs isolated by date for this manuscript are available in the supplemental material. UAS surveys of the branch region utilized for this study were conducted on July 8th, 9th, 10th, and 12th, 2018; additional information about the UAS collection metrics and processing can be found in Dietterich et al. [2021] and DeSmither et al. [2021]. Thermal images were collected every 1–3 days during the eruption and maps were constructed using a series of oblique images collected by a handheld thermal camera operated by a user in a helicopter [Patrick 2024], following

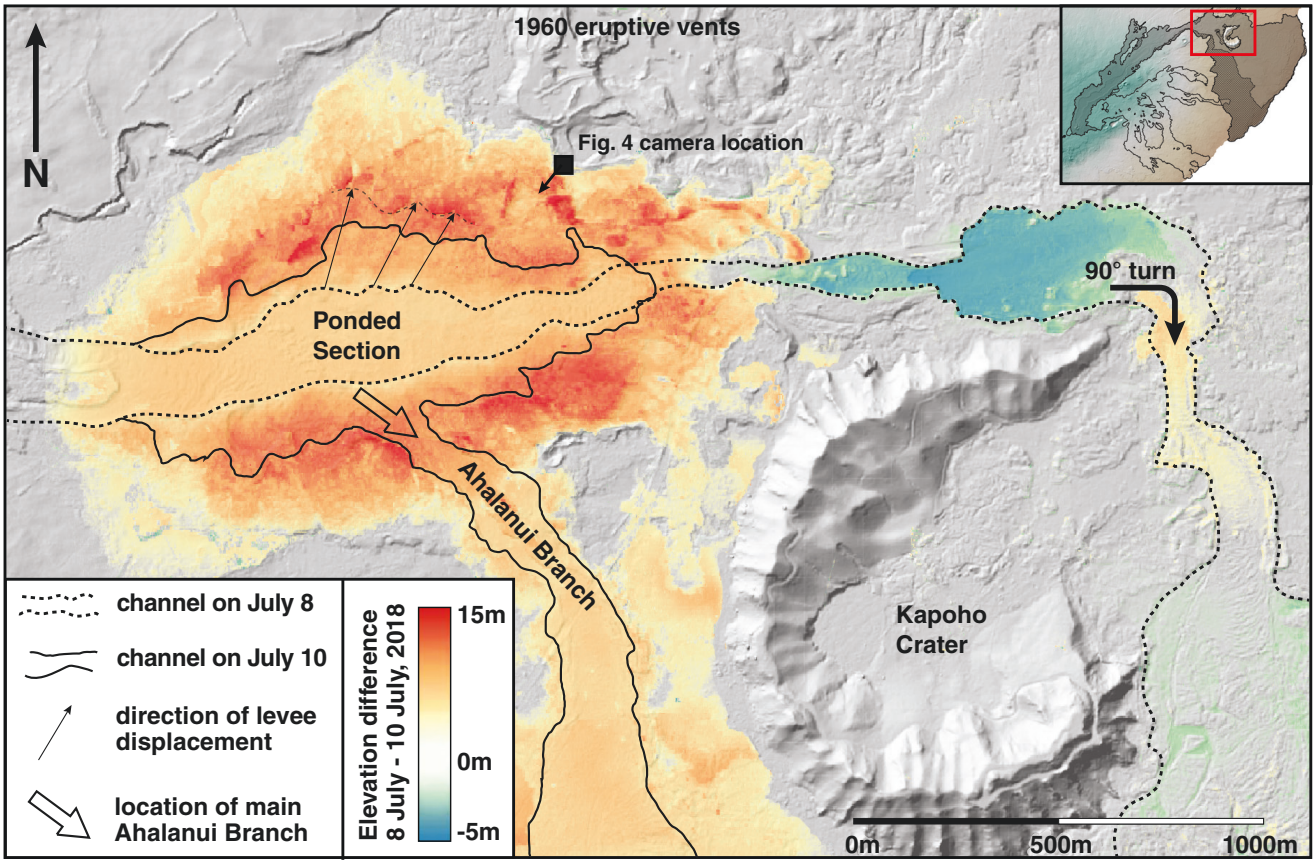

Figure 3: Elevation difference LiDAR DEMs from July 8 and 10, 2018. The open arrow indicates the location of the levee break that hosted the Ahalanui flow lobe. The small black arrows indicate the original and translated positions of levee wall sections. The dotted line shows the active channel footprint as it existed on July 8th, 2018, one day prior to the branching event, while the solid black line shows the post-branch extent of the ponded area and re-routed flow. The camera location and view angle from the video stills in Figure 4 are also noted.

the same general methodology of Patrick et al. [2017]. Field notes from U.S. Geological Survey scientists and other personnel present during the eruption were used to augment the timeline of events captured in the photo and video imagery [Patrick et al. 2024]. These daily updates identified the timing and location of events, as well as notable observations (e.g. fountain heights, relative differences between fissure intensity from day to day, etc.). The infrasound data, used to identify effusion rate pulses in this study, are from a four-element campaign array installed near the vent [Lyons et al. 2021]. We conducted an additional field survey in November 2021 to document physical properties of the levees that were not available from data collected during the eruption and to provide more context for interpreting the LiDAR survey results. We note that permission was acquired for all field work from the landowners whose properties were part of the study area.

4 Results

We present an integrated timeline of the Ahalanui branching event derived from a range of geophysical, remote sensing, and observational datasets [DeSmither et al. 2021; Shelly and Thelen 2021; Patrick 2024; Patrick et al. 2024]. Activity was relatively stable the month prior to the event and was characterized by a channel-fed flow field and ocean entry [Neal et al. 2019] (Figures 1 and 2). Instantaneous effusion rates were ~150 $m^3 s^{-1}$ during this stable period and had begun cycling daily with surges following summit collapse events, leading to channelized lava back-ups and ooze-outs that dominated the dynamics of the distal lava fan [Dietterich et al. 2021]. On the afternoon of July 8th, 2018, the day before the branching event, the ponded section covered a surface area of ~6800 m^2 and contained a minimum lava volume of 2.1 × 10^6 m^3 (Figure 3). Time-lapse camera footage, thermal imagery, field observations, UAS overflights, and a repeat-pass LiDAR survey documented dramatic changes from July 9th, 2018, and into the morning of the 10th that would rapidly redistribute much of this volume.

4.1 Timeline of the Ahalanui branching event

UAS overflight imagery collected on the morning of July 9th at 00:43 Hawaii Standard Time (HST) showed no notable deviation from the previous day's activity, with lava flowing around the northern side of Kapoho Crater. Following a period of lower effusion rate and lower channel fill level in the late hours of July 8th, the eruption rate sharply increased around

Figure 4: Video stills capturing the movement of the levees on July 9, 2018, and illustrated steps of intrusion, inflation, and destruction of perched levees (the location of the camera is shown in Figure 3). Trees in the foreground of the images are ~2 m tall and the distance to the cone in the background is 1.75km. [A] 8:30, a surge can be seen causing fires in the transition area between the braided and ponded sections. [A′] shows the levee prior to an increase in flux. Note the thermal profile and how the hot, ductile portion of the levee (red) extends beneath the structure and into the originally emplaced flow (orange). [B] 10:00, lava has deformed the levee and is starting to seep out of the flow margin. The yellow circle identifies a small feature on the edge of the levee that can be seen in images [B–D]. [B′] shows an increase in flux causing lava to intrude beneath the levees, causing them to deform vertically. [C] 13:00, lava can now be seen aggressively seeping out of the flow margin, and the identifiable plate is slightly closer to the camera. [C′] shows lava seeping even further into the levees and oozing out of weak zones, the horizontal displacement of the levees, and subsequent widening of the channel. [D] Substantial differences in the location of the seeping section are noted, the identifiable plate is much closer to the camera, and deformed and rotated levee blocks are visible. [D′] shows the rerouting of the original flow into a new branch along with the final extent of block rotation.

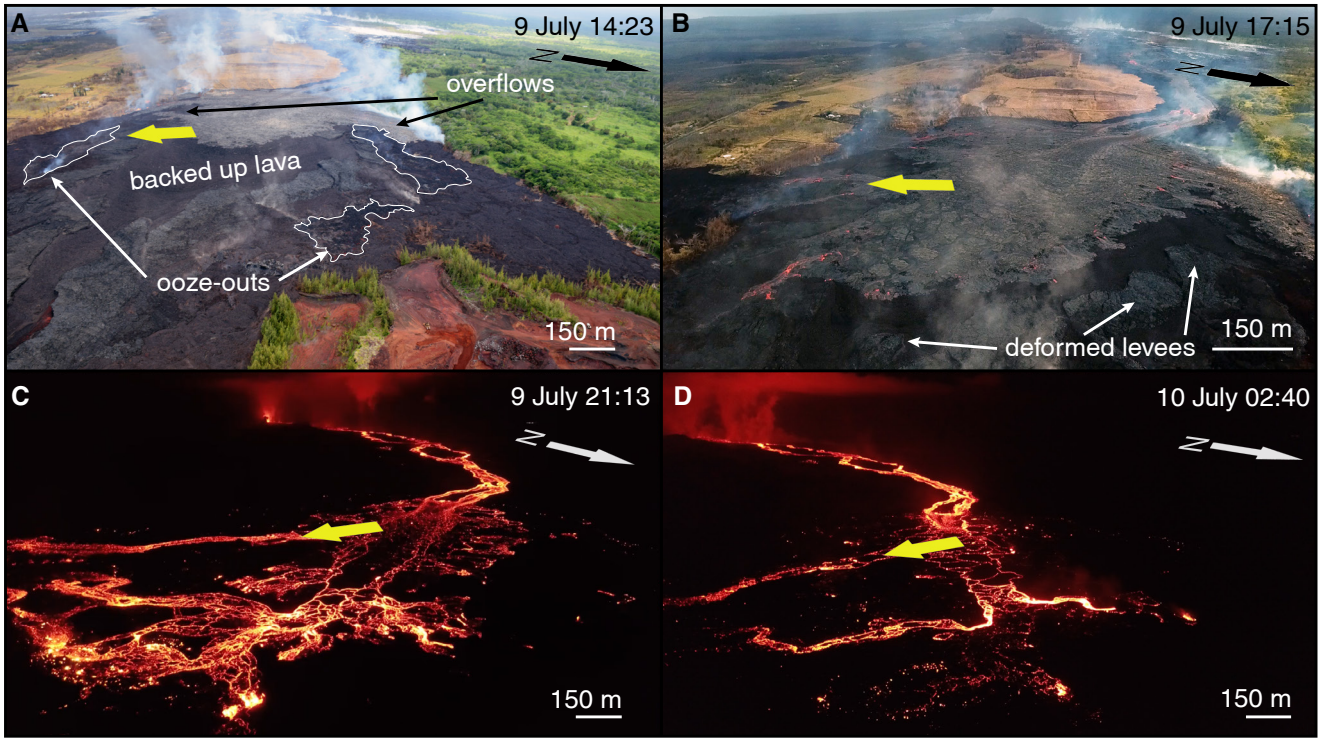

Figure 5: Evolution of the ponded section during the branching event. These aerial photos are taken from a similar view angle to the Fig. 4 webcam. [A] Image taken from an overflight that shows ooze-outs, the backed up lava in the channel, and the deformation of the pond and levees. Note how the channel in the lower left of the panel is not filled to the maximum height of the levee, indicating a blockage between it and the ponded section. The yellow arrow indicates the area where the branch eventually occurred. [B] Images from a UAS overflight later that afternoon. A surge in effusion rate led to continued overprinting of the backed up ʻaʻā. The area continued to deform throughout this time and the yellow arrow indicates where the branch has now started to form. [C] Night UAS survey showing the early stages of the Ahalanui branch. [D] Early morning UAS survey showing a drop in effusion rate, which would help establish the Ahalanui branch as the main feeder for the rest of the eruption.

midnight on the morning of July 9th, as represented by the infrasound amplitude (Figure 2), and the lava level in the distal channel began to rise at ~05:00. Small fires along the margins of the braided section, caused by overflows, were visible beginning at 07:09 in the time-lapse video footage (Supplementary Material 1).

Initial deformation of the levee was captured in time-lapse video at 07:30, when the northern side of the ponded section began to vertically rise. Lateral motion began 45 minutes later in the northwest portion of the pond (Figure 4A). The entire northern levee became decoupled from the base of the flow at 09:15, and lava began to seep out of the flow margin from the levee base (Figure 4B). At 11:00 the levee on the south side of the ponded section began to deform similarly in both the vertical and lateral directions. A second surge was visible in the time-lapse footage at ~13:00 (Figure 4C), which caused further deformation and more prominent ooze-outs from the base of the northern levee. Large, coherent levee sections were translated and rotated outward from the channel to horizontal distances of up to 180 m and 25° to the east (clockwise) (Figure 3, Figure 4D, and Supplementary Material 1). The surge that drove this pulse may have been related to a summit collapse event that occurred at 9:20 (Figure 2). Pre- and post-event LiDAR scans indicate the channel had widened by up to 228 meters during this event, with an average horizontal velocity of the levee displacement at ~21 $\mathrm{m\,hr^{-1}}$ (Figure 3). Time lapse imagery indicates that this movement occurred in two pulses and was not a steady process.

An overflight at 14:00 captured the surging active flow spilling over the backed-up lava in the inflated ponded section (Figure 2D), small overflows causing small fires along the southwest margin of the ponded section, and a blockage on the eastern side of the pond (Figure 5A). This blockage at the distal end of the pond was weak and still allowed sluggish flow underneath the rubbly, crusted pond levee into the partially-drained distal channel and around the 90° bend. Imagery captured on this overflight at 14:23 shows heavy degassing in the section where the branch would eventually occur. UAS video taken at 17:25 shows the early stages of the advancing Ahalanui lobe (Figure 5B). By 18:00 the lateral expansion of the ponded channel section had mostly ceased, and ooze-outs had stalled, but overflows continued through the evening in the newly widened section of the channel. In addition to the lateral expansion of the area, the average thickness of the lava in the ponded section rose ~5 m between the 8th and 10th. The volume of lava in the ponded section was at least ~$3.6 \times 10^6\,\mathrm{m^3}$ at this point, a ~75 % increase from the previous day. We note that this value does not include

the ~0.9 × 10^6 m^3 contained in seeps, ooze-outs, or overflows, which was also calculated from the LiDAR data (Figure 3). A UAS overflight conducted at 21:13 shows three small lobes advancing from the south side of the ponded section, with the western-most being the dominant of the three and extending ~750 m from the pond—this lobe would go on to become the Ahalanui branch (Figure 5C and 5D).

By 06:00 on the morning of July 10th, 2018, the effusion rate had decreased and flow in the ponded section had focused mostly into the nascent Ahalanui lobe (Figure 2E and Figure 5D). The flow length from the branch point reached 2.5 km by 13:00 PM HST. The level of fill dropped by 8 m in the original channel that routed along the northeast side of Kapoho Crater (Figure 3). Supply to the ocean entry was still fed by the draining of the abandoned and latent supply in the distal fan, although these points waned over the next few days.

5 Discussion

We identify several specific elements that influenced the catastrophic failure of the levee and frame the discussion in the context of how some of those elements propagated from the summit and into the lower East Rift Zone, and subsequently from the vent to the branch location. Finally, we describe the impacts of the relationships between these elements as part of a broader understanding of how to better identify and monitor the hazards that exist along the sides of lava flows.

5.1 Topographic influence on channel geometry

Topography was one of the most important factors in the levee failure because, at the highest level, it dictates the morphology of the lava flow; without a channelized flow and slope breaks, the conditions that resulted in the levee failure would not exist. Other studies that document levee failures observed that they generally occurred in areas where the width of the channel changes rapidly over short distances [Hyman et al. 2022; Orr et al. 2022]. The pre-eruptive topography between the braided and ponded sections transitioned from a slope of 5–10° to 0.5° (Figure 1). Areas of low slope promote a greater degree of lateral spreading [Gregg and Fink 2000; Dietterich and Cashman 2014], and the slope-break and flat topography in this section resulted in a widening of the flow from 150–215 m to >800 m during the initial advance. The extent of spread in this area was controlled along both the northern and southern margins by the Kapoho and Koa'e faults, which were inactive during the eruption (Figure 6). This area provided a prime location for future failure because it did not facilitate the building of narrow, bounding levees early in the eruption, as it had upchannel, and because the graben provided an area where the lava flow was able to locally thicken.

The initial channel just downslope from the ponded section was narrow and buttressed against a lava flow emplaced during an eruption in 1960 and Kapoho Crater (Figure 6). The morphology of the 1960 flow in this area is complex because it corresponds with a natural graben and artificial lava impoundment structures, which had caused the 1960 flow to pond and thicken locally upslope from the barriers [MacDonald 1962; Dietterich et al. 2015]. This morphology influenced the fissure 8 flow channel in three important ways: 1) Confinement of the 2018 flow between the 1960 flow margin and Kapoho Crater produced an abnormally narrow channel within a region of shallow underlying slope, 2) the flow was directed around a sharp 90° bend in this confined terrain, and 3) the topography paved over in 1960 results in a locally shallow slope, which promoted additional ponding just upslope of this sharp bend on the north side of Kapoho Crater (Figure 6). These elements are important for branching because the narrowing of the channel in this section created favorable conditions for both upstream ponding and down-channel blockages.

5.2 Influence of lava supply and rheology

Of equal importance to the topography is the volume and rate of lava supply from the vent, as variable effusion rates influence the formation of channelized flows and their transition to compound flow fields from branching behavior [Dietterich and Cashman 2014]. Effusion rates are difficult to accurately estimate continuously throughout an eruption [Harris et al. 2007], and several methods were employed to observe them for the 2018 eruption [Dietterich et al. 2022]. The time averaged discharge rate was ~100–200 m^3s^{-1} in late-May/early-June, when the fissure 8 flow was establishing an open channel and lava delta that, collectively, reached 13.25 km to the ocean [Dietterich et al. 2022]. Infrasound energy and instantaneous effusion rate data strongly correlate, and both show a peak in effusion rate in mid-June of ~350 m^3s^{-1}, followed by a gradual decline to ~250 m^3s^{-1}, best seen in the infrasound from late June through the second week of July [Dietterich et al. 2021] (Figure 2). This reduced output, when combined with the stalling of the flow as it encountered the lower slope of the flat coastal area and ocean entry, led to the upslope migration of the transitional channel zone within the channel (Figure 2). The transition zone, which indicates a rheological change in lava from purely viscous to complex viscoplastic behavior associated with increasing crystallinity and viscosity [Cashman et al. 1999], was located in a narrow portion of the channel near the 90° turn on July 8th and retreated upchannel towards the ponded section by the afternoon of July 9th.

Channelized flows that are obstructed are more prone to failure due to back ups and pressure transients, and the increase in viscosity and viscoplastic behavior across this transition will result in a more sluggish response to flow [e.g. Peterson and Tilling 1980]. The broad decline in effusion rate from late June through mid July was regularly disrupted by the cycles of surges driven by summit caldera collapse events, which had a significant impact on the levee failure [Patrick et al. 2020; Dietterich et al. 2021; Lyons et al. 2021; Dietterich et al. 2022]. These large oscillations in effusion would double the volumetric flux through the channel over the course of a few hours from ~250 m^3s^{-1} to ~500 m^3s^{-1} [Patrick et al. 2019], driving pressure transients that could propagate as surges in flux from the vent to the ponded area in as little as ~3 hours [Patrick et al. 2019].

When the transitional channel zone was located in the distal fan, the volume increase from surges could be accommodated in the network of ephemeral tubes that fed the lava supply

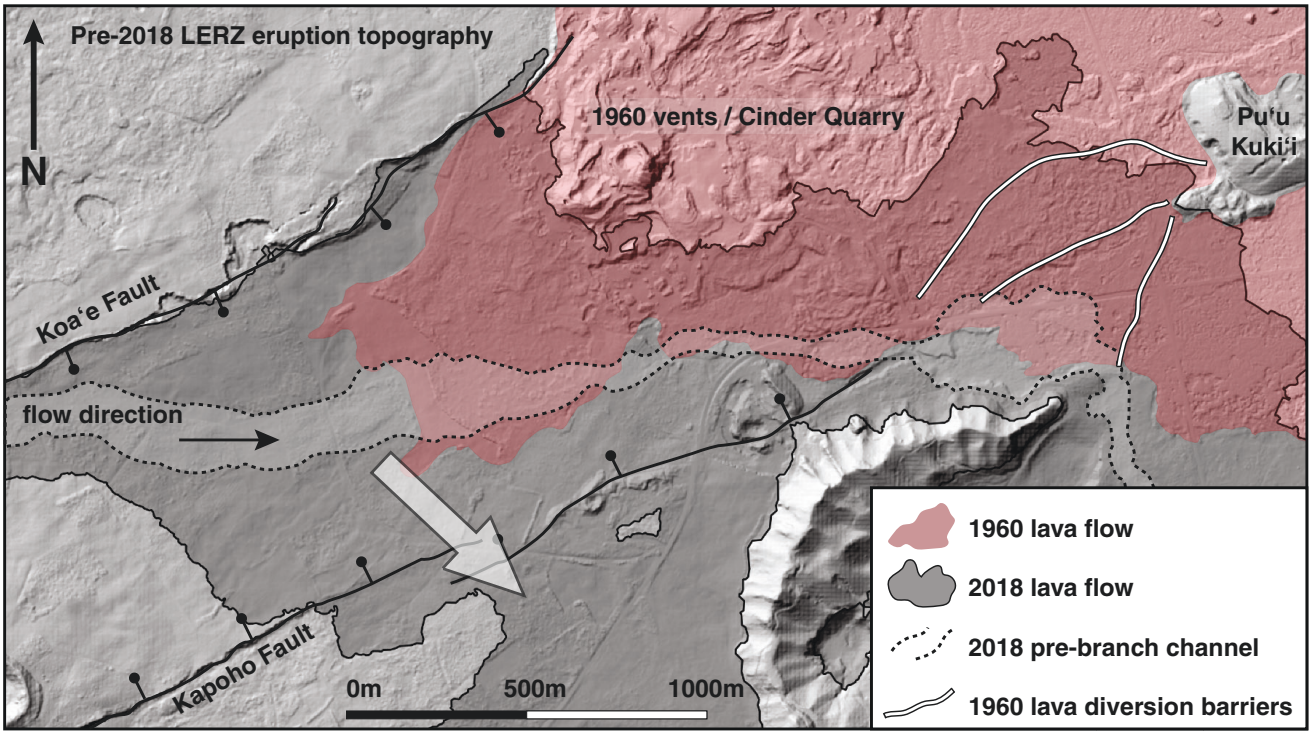

Figure 6: Pre-2018 eruption topography (light gray shading) with the locations of local topographic features. The areas of the 1960 (red) and 2018 (dark gray) lava flows are shown, as well as the pre-Ahalanui branch active channel (dashed line) and lava diversion structures built during the 1960 eruption to impound advancing lava (white lines). The shaded gray arrow shows the area where the branch initiated from within the ponded section.

throughout the fan. Once the zone migrated into the confined channel along the north side of Kapoho Crater, subsequent surges were slowed by the higher viscosity and yield strength of the ʻaʻā, without a broad flow to disperse through, leading to overflows and seeps in the ponded section; these seeps deformed the levees to the extent that they failed, causing the flow to divert into the Ahalanui branch (Supplementary Material 1). A levee formed at the distal end of the pond across the outlet to the narrow original channel, although reduced flow continued beneath it for ~24 hours.

Following a summit caldera collapse event at 02:54 on July 8th, infrasound energy records only a minor post-collapse surge at the vent, before later growing steeply and peaking around midnight on July 9th. This spike in infrasound is consistent with a spike in effusion rate at the vent that propagated a surge down the channel in the early hours of July 9th, independent of a summit collapse event. This surge likely induced the seeps that led to the destabilization of the levees captured in the webcam imagery. A summit caldera collapse event then occurred at 09:20 AM HST, followed by a smaller rise in infasound energy associated with a surge, which resulted in the acceleration of levee deformation that would ultimately lead to failure later in the day. Overflows that accompanied this second surge event ignited fires adjacent to the channel that were still active several hours later and observed during a helicopter overflight (Figure 5, Supplementary Material 1). It is unlikely that these small surges would have caused the levee to fail individually, but collectively they were able to create a pressure transient within the ponded section that exceeded the strength of the levees.

5.3 Levee construction

The few studies on bottom-up structural failures identify a critical minimum overpressure value [Patrick and Orr 2012; Orr et al. 2022]. The levees in the ponded section of the 2018 channel were 15–20 m tall at the time of the failure and we calculate a range of passive overpressures of 4.0 to 5.3 bar, assuming hydrostatic pressure in the channel, that is, $P = \rho g h$, where ρ is the lava density, g is the gravitational constant, and h is the depth of the lava. Several collapses at rootless vents in 2008 during the Puʻuʻoʻo eruption were studied; a maximum shield height of 20–30 m was reached when basal breakouts occurred, and overpressures of 5–7 bar were calculated to be necessary for breakouts to extrude through the shield walls [Patrick and Orr 2012]. We note that the levees also exceeded 15 m in the vent-proximal perched section, which indicates that levee height and pressure build up alone cannot be the sole cause of structural failure.

How the failure propagated from the base of the levees in the ponded section provides additional insight into how the levee's construction may increase their susceptibility to fail (Supplementary Material 1). As the flow was initially emplacing in early June, thick ʻaʻā levees formed at the flow margins behind the flow front; this is an important part of the channelization process and has been described in detail in many other studies [Sparks et al. 1976; Lipman and Banks 1987; Bailey et

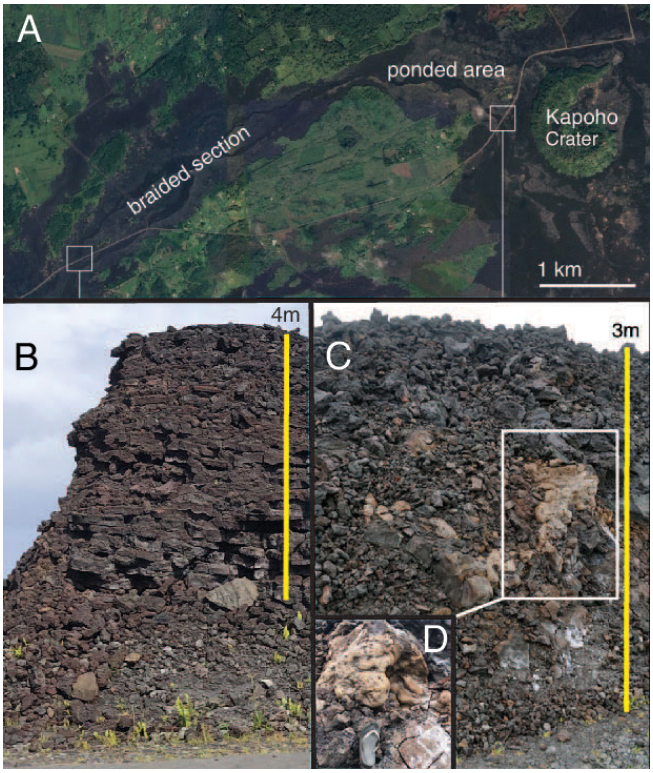

Figure 7: Cross-sections of levee walls. [A] Overview map indicating the location of levee road cuts. Image data: Airbus, TerraMetrics, and MBARI. [B] Levee cross-section from the braided section, which experienced repeated overflows. [C] Levee cross-section cross-section from the ponded area, where the Ahalanui branch formed. [D] A zoomed in view of lavas that were fluid for an extended period of time, as indicated by the smoother texture, as well as a higher density than the adjacent rubble, both a result of extensive degassing.

al. 2006; Favalli et al. 2010; Harris et al. 2022]. The rubbly levees that confined the wide fluid-filled zone of dispersed flow were 800–1250 m wide on June 4th and progressively crusted over and localized into a stable open channel 140–200 m wide by mid-June, with marginal zones of molten, but sluggish flow [Zoeller et al. 2019]. Progressive overflows 10s of cm in thickness built up the levees and extended up to 100 m laterally across the stable channel margins. These pāhoehoe stacks acted as an insulator for the molten core still contained within the underlying ʻaʻā flows. On July 9th, this still-fluid basal ʻaʻā levee interior offered the pathway for lava at the channel base to inflate and ooze-out from underneath the stacks of cold, thin pāhoehoe sheets, rafting and translating the levee blocks away as the flow burst apart [Patrick et al. 2024].

Post-eruptive field examination of the preserved levees records this levee construction history. Modeling of the temperature field in lava flow levees has assumed a homogenous construction [Quareni et al. 2004], although field studies indicate a substantially more complicated interior [Sparks et al. 1976; Harris et al. 2009; 2022]. Highway 132, which was crossed by the fissure 8 flow in several places, was rebuilt after the eruption and exposes the top ~5 m of the levees in cross section (Figure 7). These roadcuts show the exposed portions of the levees are built up from numerous overflow units; the levees in the ponded section were 15–20 m tall and were likely built from 15+ overflow units. These same roadcuts expose less developed levees down-channel that contain a rubbly and fluid interior core, similar to what would have been emplaced as part of the initial flow advance (Figure 7). An intact portion of the translated levee on the north side of the ponded section was examined and shows numerous overflow units capping a more disorganized layer. We suggest that the levees in the ponded section contained a basal unit with a partially fluid interior that was thermally insulated by repeated pāhoehoe overflows, which provided an ideal environment for lava seeps to undermine the levee from the base due to the hydraulic connection with the active channel. Similar features were observed during the 1984 eruption of Mauna Loa [Lipman and Banks 1987], although we note that they did not result in levee failure. In addition to this deformable core, several weak spots were “inherited” from heterogeneities in the flow structure during its initial advance; a small arm that inundated the area to the southwest of Kapoho Crater in early June but was quickly abandoned was the same location where the levee failed, forming the Ahalanui Branch (Figures 1, 3, and 4). Similarly, levee inflation and ooze-outs in this ponded zone were visible in response to the final surge of the eruption on August 2nd [Patrick et al. 2024].

5.4 Synthesis of contributing causes and cascading effects

Eruptions evolve in a cascading manner that can be difficult to forecast and focused research on the relationships between the processes that prime them will better prepare volcano observatory scientists for future eruptions [Patrick et al. 2020]. Establishing the sequential order of events and their impact on the branching process provides the necessary components to aid in future hazard assessment for levee failures. The flow encountered shallower topography as it advanced into the Kapoho region on June 2nd and widened in this area. A small lobe broke out on the southern margin on June 3rd by crossing the low drainage divide and following the local line of steepest descent. Sufficient lava supply and fluctuating effusion over the next month built up the levees along the channel, to heights of >15 m in many places. A gradual decline in effusion rate at the end of June caused the transitional channel zone to migrate up the open channel from the distal fan. The ephemeral supply network in the fan accommodated surges through lateral ooze-outs at the margins of the fan. However, once the channel backed-up to the 90° turn section in early July, it became confined with fewer drainage points. Effusion rate continued to fluctuate for several days, until it began declining steadily on July 7th into the morning of July 9th. An observed increase in effusion rate at the vent in the early morning hours on July 9th sent a surge of lava down the channel. This surge reached the lower-sloped ponded area and began to stall and slow, an effect enhanced by sluggish flow of the more viscous lava with increased yield strength at the transitional channel zone in the narrow, confined channel downslope. This combined effect of an increase in viscosity and yield strength across the confined portion of the channel led to a build-up of lava in the ponded section

and the intrusion of lava into the base of the levees, which initiated deformation. The point of failure was the same location as the breakout on June 3rd, suggesting the original ʻaʻā levee was inherently weaker in this location and primed to fail again, given the right conditions. Once this more catastrophic failure occurred, the flow was permanently re-routed and new areas were quickly inundated by lava. Ultimately, we find that this event was due to the confluence of many elements and was not the result of a single contribution.

5.5 Implications for hazard assessment

Insights from this event can inform operational hazard assessment, monitoring, and data collection during future eruptions. During the 2018 eruption, initial forecasting of the fissure 8 flow demonstrated the potential for flow branching overcoming the graben boundary drainage divide in this region, with the June 6th southern flow breakout extents matching an earlier forecast from May 29th. However, the potential of the region to fail again, once apparently stable, was not anticipated at the time. Our analysis reveals key factors that combined to increase the likelihood of a levee failure in this location and the early signs of deformation that preceded whole-sale branching. Syn-eruptive monitoring and analysis of these factors and signals could better characterize the localized hazard in similar locations during future eruptions and be used to inform deployment of instruments to monitor the signs of potential failure (e.g. webcams, ground-based radar, or other sensors to detect surges, levee inflation, and ooze-outs) to generate failure alerts [Dietterich and Neal 2022].

Areas where primary branching occurs and lobes are abandoned early in the flow's emplacement should be noted and monitored; this is especially true if the area is flat and corresponds to drainage divides where a breakout could generate a new flow branch. Places that failed or branched before are primed to fail again, under the right circumstances, and eruption monitoring should include repeat visits to these sites to capture any signs of precursory deformation or minor ooze-outs/seeps. Oscillations in effusion rate are another factor; if possible, instruments that provide consistent data on relative trends, such as infrasound, should be deployed near the vent. Repeat surge cycles have been shown to induce seeps in earthen levees [Jadid et al. 2020], and we observe similar behavior here. While surges alone are not likely to cause a failure event by themselves, they do build the heights of the levees to generate perched channels, which, when combined with blockages or localized increases in the internal viscosity of the flow, create a favorable environment for failure due to increasing flow thickness and thus pressurization of the system. Monitoring the channel for blockages, particularly at locations where the channel narrows or back-ups and crusts over, could help forecast events like this and those of the Mauna Loa 1984 [Lipman and Banks 1987] and 2022 flows [Dietterich et al. 2023]. The transitional channel zone is also an important factor for levee failure because it defines the initial levee structure (e.g. rubbly levees with molten core), the style of secondary overflows (here, thin pāhoehoe sheets), and the down-channel transition in rheology to a higher-viscosity fluid with a yield strength that is more resistant to flow. These elements all likely played a role in the instability of the distal ponded channel segment, and thus this transition should be considered as an area of locally increased hazard. Redefining hazard zones is especially critical when we consider the volume stored in wider parts of a channel and their inundation potential for distal areas because hydraulic head and stored volume will dictate how far and fast a "dam-break" style breakout propagates [Lyman et al. 2005]. Therefore, areas where channel widths pinch and swell over a short distance should be monitored during eruptions [Harris et al. 2022].

Our findings represent a critical component needed to advance lava flow models. Lava flow models are currently only able to simulate branching events that occur as flows advance and not those that occur due to structural failures. Oscillations in effusion rate are necessary to recreate perched features and future developments in lava flow modeling should attempt to model levee construction in addition to the initial sheet advance. Only when this is a regular feature of these codes can levee breach modeling be attempted based on simplified channel pressure estimates. Recent advances in forecast model development have enabled the modeling of self channelization and levee formation [Hyman et al. 2022]; however, integrating these methods with accurate estimates of variable supply rate and the rheological transitional channel zone remain a theoretical as well as technical challenge.

6 Conclusions

We reconstructed the events leading up to the July 9, 2018, channel breach that led to the rerouting of the primary 2018 lava channel and the inundation of 5.7 km^2, including an additional 86 built structures and Ahalanui Beach Park. The confluence of several elements played a role in the growth and failure of the levee: 1) pre-existing topography, 2) large oscillations in effusion rate, 3) rheology, and 4) construction and structure of the levees. Our results identify features and changes in activity that may be monitored during effusive eruptions to potentially forecast and model later-stage flow branching events. This in-depth reconstruction of the event will be helpful to those managing crises during similar eruptions and provides useful insights that can help advance lava flow inundation forecasting models.

Author Contributions

EG participated in all non-eruption response phases of this work. HD contributed to the development of the study, participated in the eruption response and field work, and provided effusion rate data. MP participated in the eruption response and field work, contributed to the development of the study, and processed the thermal imagery data. DH contributed to the discussion and participated in field work. BC participated in field work. JL processed and provided the infrasound data. EM processed and provided damage report data. All authors reviewed the manuscript.

Acknowledgements

Mahalo nui loa to the local landowners for permitting us access to the field sites. This work was funded by NSF Award: 1952646 EAR-PF (PI: Gallant) and by Additional Supplemen-

tal Appropriations for Disaster Relief Act of 2019 (H.R. 2157). We also thank the editor, O. Chevrel and reviewers S. Peters, T. Orr, and an anonymous individual for comments that improved the quality of this manuscript. Any use of trade, firm, or product names is for descriptive purposes only and does not imply endorsement by the U.S. Government.

Data Availability

All imagery and monitoring data used in this manuscript are public domain and available from the U.S. Geological Survey through the Science-Base data releases cited in this paper.

Copyright notice

References

Applegarth, L. J., M. R. James, B. Van Wyk de Vries, and H. Pinkerton (2010). "Influence of surface clinker on the crustal structures and dynamics of ʻaʻā lava flows". *Journal of Geophysical Research: Solid Earth* 115(B7). DOI: 10.1029/2009JB006965.

Bailey, J. E., A. J. L. Harris, J. Dehn, S. Calvari, and S. K. Rowland (2006). "The changing morphology of an open lava channel on Mt. Etna". *Bulletin of Volcanology* 68(6), pages 497–515. DOI: 10.1007/s00445-005-0025-6.

Belousov, A. and M. Belousova (2018). "Dynamics and viscosity of ʻaʻā and pahoehoe lava flows of the 2012–2013 eruption of Tolbachik volcano, Kamchatka (Russia)". *Bulletin of Volcanology* 80, pages 1–23. DOI: 10.1007/s00445-017-1180-2.

Branca, S., E. De Beni, and C. Proietti (2013). "The large and destructive 1669 AD eruption at Etna volcano: reconstruction of the lava flow field evolution and effusion rate trend". *Bulletin of Volcanology* 75, pages 1–16. DOI: 10.1007/s00445-013-0694-5.

Burgi, P.-Y., G. Boudoire, F. Rufino, K. Karume, and D. Tedesco (2020). "Recent activity of Nyiragongo (Democratic Republic of Congo): New insights from field observations and numerical modeling". *Geophysical Research Letters* 47(17), e2020GL088484. DOI: 10.1029/2020GL088484.

Cashman, K. V., C. Thornber, and J. P. Kauahikaua (1999). "Cooling and crystallization of lava in open channels, and the transition of Pāhoehoe Lava to ʼAʻā". *Bulletin of Volcanology* 61(5), pages 306–323. DOI: 10.1007/s004450050299.

Chevrel, M. O., A. Harris, A. Peltier, N. Villeneuve, D. Coppola, M. Gouhier, and S. Drenne (2022). "Volcanic crisis management supported by near real-time lava flow hazard assessment at Piton de la Fournaise, La Réunion". *Volcanica* 5(2), pages 313–334. DOI: https://doi.org/10.30909/vol.05.02.313334.

Culha, C., S. Spinner, and J. Suckale (2023). "The Yih instability in layered lava flow may initiate the pāhoehoe to ʻaʻā lava transition". *Geophysical Research Letters* 50(10), e2022GL101302. DOI: 10.1029/2022GL101302.

Del Negro, C., A. Cappello, M. Neri, G. Bilotta, A. Hérault, and G. Ganci (2013). "Lava flow hazards at Mount Etna: constraints imposed by eruptive history and numerical simulations". *Scientific Reports* 3(1), page 3493. DOI: 10.1038/srep03493.

DeSmither, L., A. Difenback, and H. R. Dietterich (2021). "Unoccupied Aircraft Systems (UAS) video of the 2018 summit eruption of Kīlauea Volcano, Hawai'ʻi". *U.S. Geological Survey Data Release* 47(17), e2020GL088484. DOI: 10.5066/P9MYKFWB..

Di Fiore, F., A. Vona, S. Kolzenburg, S. Mollo, and C. Romano (2021). "An extended rheological map of pāhoehoe—ʼaʻā transition". *Journal of Geophysical Research: Solid Earth* 126(7), e2021JB022035. DOI: 10.1029/2021JB022035.

Dietterich, H. R. and K. V. Cashman (2014). "Channel networks within lava flows: Formation, evolution, and implications for flow behavior". *Journal of Geophysical Research: Earth Surface* 119(8), pages 1704–1724. DOI: 10.1002/2014JF003103.

Dietterich, H. R., K. V. Cashman, A. C. Rust, and E. Lev (2015). "Diverting lava flows in the lab". *Nature geoscience* 8(7), pages 494–496. DOI: 10.1038/ngeo2470.

Dietterich, H. R., A. K. Diefenbach, S. A. Soule, M. H. Zoeller, M. R. Patrick, J. J. Major, and P. R. Lundgren (2021). "Lava effusion rate evolution and erupted volume during the 2018 Kīlauea lower East Rift Zone eruption". *Bulletin of Volcanology* 83, pages 1–18. DOI: 10.1007/s00445-021-01443-6.

Dietterich, H. R., G. E. Grant, B. Fasth, J. J. Major, and K. V. Cashman (2022). "Can Lava Flow Like Water? Assessing Applications of Critical Flow Theory to Channelized Basaltic Lava Flows". *Journal of Geophysical Research: Earth Surface* 127(9), e2022JF006666. DOI: https://doi.org/10.1029/2022JF006666.

Dietterich, H. R. and C. A. Neal (2022). "A look ahead to the next decade at US volcano observatories". *Bulletin of Volcanology* 84(6). DOI: 10.1007/s00445-022-01567-3.

Dietterich, H. R., M. R. Patrick, M. Zoeller, D. Hyman, F. Trusdell, N. Deligne, D. Downs, E. Gallant, K. Lynn, C. Parcheta, T. Orr, J. Schmith, J. Chang, B. Walker, K. Mulliken, L. DeSmither, B. Andrews, M. Grismer, K. Cashman, A. Mosbrucker, J. Ball, and P. Lundgren (2023). "Observations and insights into lava flow emplacement dynamics during the Mauna Loa 2022 eruption". *International Association of Volcanology and Chemistry of the Earth's Interior (IAVCEI) Scientific Assembly 2023*. Rotorua, New Zealand.

Favalli, M., A. Fornaciai, F. Mazzarini, A. Harris, M. Neri, B. Behncke, M. T. Pareschi, S. Tarquini, and E. Boschi (2010). "Evolution of an active lava flow field using a multitemporal LIDAR acquisition". *Journal of Geophysical Research: Solid Earth* 115(B11). DOI: 10.1029/2010JB007463.

Gansecki, C., R. L. Lee, T. Shea, S. P. Lundblad, K. Hon, and C. Parcheta (2019). "The tangled tale of Kīlauea's 2018 erup-

tion as told by geochemical monitoring". *Science* 366(6470), eaaz0147. DOI: 10.1126/science.aaz0147.

Gregg, T. K. and J. H. Fink (2000). "A laboratory investigation into the effects of slope on lava flow morphology". *Journal of Volcanology and Geothermal Research* 96(3-4), pages 145–159. DOI: 10.1016/S0377-0273(99)00148-1.

Guest, J., C. Kilburn, H. Pinkerton, and A. Duncan (1987). "The evolution of lava flow-fields: observations of the 1981 and 1983 eruptions of Mount Etna, Sicily". *Bulletin of Volcanology* 49, pages 527–540. DOI: 10.1007/BF01080447.

Harris, A. J. L., J. Dehn, and S. Calvari (2007). "Lava effusion rate definition and measurement: a review". *Bulletin of Volcanology* 70, pages 1–22. DOI: 10.1007/s00445-007-0120-y.

Harris, A. J. L., M. Favalli, F. Mazzarini, and C. W. Hamilton (2009). "Construction dynamics of a lava channel". *Bulletin of Volcanology* 71, pages 459–474. DOI: 10.1007/s00445-008-0238-6.

Harris, A. J. L., S. K. Rowland, and M. O. Chevrel (2022). "The anatomy of a channel-fed ʻaʻā lava flow system". *Bulletin of Volcanology* 84(7), page 70. DOI: 10.1007/s00445-022-01578-0.

Harris, A. J. L., N. Villeneuve, A. Di Muro, V. Ferrazzini, A. Peltier, D. Coppola, M. Favalli, P. Bachèlery, J.-L. Froger, L. Gurioli, et al. (2017). "Effusive crises at Piton de la Fournaise 2014–2015: a review of a multi-national response model". *Journal of Applied Volcanology* 6(1), pages 1–29. DOI: 10.1186/s13617-017-0062-9.

Hon, K., C. Gansecki, and J. Kauahikaua (2003). "The transition from ʻa ʻā to pāhoehoe crust on flows emplaced during the Pu ʻu ʻŌ ʻō-Kūpaianaha eruption". *The Puʻu ʻŌʻō-Kūpaianaha Eruption of Kīlauea Volcano, Hawaiʻi: The First 20 Years*. Edited by C. Heliker, D. A. Swanson, and T. J. Takahashi. Volume 1676. US Government Printing Office, pages 89–104. U.S. Geological Survey Professional Paper.

Hyman, D. M., H. R. Dietterich, and M. R. Patrick (2022). "Toward Next-Generation Lava Flow Forecasting: Development of a Fast, Physics-Based Lava Propagation Model". *Journal of Geophysical Research: Solid Earth* 127(10), e2022JB024998. DOI: 10.1029/2022JB024998.

Jadid, R., B. M. Montoya, V. Bennett, and M. A. Gabr (2020). "Effect of repeated rise and fall of water level on seepage-induced deformation and related stability analysis of Princeville levee". *Engineering Geology* 266, page 105458. DOI: 10.1016/j.enggeo.2019.105458.

Jenkins, S. F., S. Day, B. Faria, and J. Fonseca (2017). "Damage from lava flows: insights from the 2014–2015 eruption of Fogo, Cape Verde". *Journal of Applied Volcanology* 6(1), pages 1–17. DOI: 10.1186/s13617-017-0057-6.

Lipman, P. W. and N. G. Banks (1987). "AA flow dynamics, Mauna Loa 1984". *Volcanism in Hawaii*. Edited by R. W. Decker, T. L. Wright, and P. H. Stauffer. Volume 1350. Washington, D.C.: HVO, pages 1527–1567. U.S. Geological Survey Professional Paper.

Lockwood, J., N. Banks, T. English, P. Greenland, D. Jackson, D. Johnson, B. Koyanagi, K. McGee, A. Okamura, and M. Rhodes (1985). "The 1984 eruption of Mauna Loa Volcano, Hawaii". *Eos, Transactions American Geophysical Union* 66(16), pages 169–171. DOI: 10.1029/eo066i016p00169-01.

Lormand, C., A. J. Harris, M. O. Chevrel, S. Calvari, L. Gurioli, M. Favalli, A. Fornaciai, and L. Nannipieri (2020). "The 1974 west flank eruption of Mount Etna: a data-driven model for a low elevation effusive event". *Frontiers in Earth Science* 8, page 590411. DOI: 10.3389/feart.2020.590411.

Lyman, A. W., R. C. Kerr, and R. W. Griffiths (2005). "Effects of internal rheology and surface cooling on the emplacement of lava flows". *Journal of Geophysical Research: Solid Earth* 110(B8). DOI: 10.1029/2005jb003643.

Lyons, J. J., H. R. Dietterich, M. R. Patrick, and D. Fee (2021). "High-speed lava flow infrasound from Kīlauea's fissure 8 and its utility in monitoring effusion rate". *Bulletin of Volcanology* 83, pages 1–12. DOI: 10.1007/s00445-021-01488-7.

MacDonald, G. A. (1962). "The 1959 and 1960 eruptions of Kilauea volcano, Hawaii, and the construction of walls to restrict the spread of the lava flows". *Bulletin Volcanologique* 24, pages 249–294.

Meredith, E. S., S. F. Jenkins, J. L. Hayes, N. I. Deligne, D. Lallemant, M. R. Patrick, and C. Neal (2022). "Damage assessment for the 2018 lower East Rift Zone lava flows of Kīlauea volcano, Hawaiʻi". *Bulletin of Volcanology* 84(7), page 65. DOI: 10.1007/s00445-022-01568-2.

Neal, C. A., S. Brantley, L. Antolik, J. Babb, M. Burgess, K. Calles, M. Cappos, J. Chang, S. Conway, L. Desmither, et al. (2019). "The 2018 rift eruption and summit collapse of Kīlauea Volcano". *Science* 363(6425), pages 367–374. DOI: 10.1126/science.aav7046.

Orr, T. R., E. W. Llewellin, and M. R. Patrick (2022). "Development, structure, and behavior of a perched lava channel at Kīlauea Volcano, Hawaiʻi, during 2007". *Journal of Volcanology and Geothermal Research* 430, page 107637. DOI: 10.1016/j.jvolgeores.2022.107637.

Pankhurst, M. J., J. H. Scarrow, O. A. Barbee, J. Hickey, B. C. Coldwell, G. K. Rollinson, J. A. Rodríguez-Losada, A. M. Lorenzo, F. Rodríguez, W. Hernández, et al. (2022). "Rapid response petrology for the opening eruptive phase of the 2021 Cumbre Vieja eruption, La Palma, Canary Islands". *Volcanica* 5(1), pages 1–10. DOI: 10.30909/vol.05.01.0110.

Patrick, M. R. (2024). "Thermal maps of the 2018 lower East Rift Zone eruption of Kīlauea Volcano, Island of Hawaiʻi". *U.S. Geological Survey data release*. DOI: 10.5066/P9C8W3NT.

Patrick, M. R., H. R. Dietterich, J. J. Lyons, A. K. Diefenbach, C. Parcheta, K. R. Anderson, A. Namiki, I. Sumita, B. Shiro, and J. P. Kauahikaua (2019). "Cyclic lava effusion during the 2018 eruption of Kīlauea Volcano". *Science* 366(6470), eaay9070. DOI: 10.1126/science.aay9070.

Patrick, M. R., B. F. Houghton, K. R. Anderson, M. P. Poland, E. Montgomery-Brown, I. Johanson, W. Thelen, and T. Elias (2020). "The cascading origin of the 2018 Kīlauea eruption and implications for future forecasting". *Nature Communications* 11(1), page 5646. DOI: 10.1038/s41467-020-19190-1.

Patrick, M. R., K. P. Kamabayashi, and R. L. Lee (2024). "Time-lapse camera and webcam images of the fissure 8 lava flow during the 2018 lower East Rift Zone eruption of Kīlauea volcano, Island of Hawai'i". *U.S. Geological Survey Data Release*. DOI: 10.5066/P9SCU4RE.

Patrick, M. R., T. Orr, G. Fisher, F. Trusdell, and J. Kauahikaua (2017). "Thermal mapping of a pāhoehoe lava flow, Kīlauea Volcano". *Journal of Volcanology and Geothermal Research* 332, pages 71–87. DOI: 10.1016/j.jvolgeores.2016.12.007.

Patrick, M. R. and T. R. Orr (2012). "Rootless shield and perched lava pond collapses at Kīlauea Volcano, Hawai'i". *Bulletin of Volcanology* 74, pages 67–78. DOI: 10.1007/s00445-011-0505-9.

Pedersen, G., A. Höskuldsson, T. Dürig, T. Thordarson, I. Jonsdottir, M. Riishuus, B. Óskarsson, S. Dumont, E. Magnússon, M. T. Gudmundsson, et al. (2017). "Lava field evolution and emplacement dynamics of the 2014–2015 basaltic fissure eruption at Holuhraun, Iceland". *Journal of Volcanology and Geothermal Research* 340, pages 155–169. DOI: 10.1016/j.jvolgeores.2017.02.027.

Peters, S., A. B. Clarke, and E. Rader (2022). "The effects of unsteady effusion rates on lava flow emplacement: Insights from laboratory analogue experiments". *Journal of Volcanology and Geothermal Research* 432, page 107674. DOI: 10.1016/j.jvolgeores.2022.107674.

Peterson, D. W. and R. I. Tilling (1980). "Transition of basaltic lava from pahoehoe to aa, Kilauea Volcano, Hawaii: field observations and key factors". *Journal of Volcanology and Geothermal Research* 7(3-4), pages 271–293.

Quareni, F., A. Tallarico, and M. Dragoni (2004). "Modeling of the steady-state temperature field in lava flow levées". *Journal of Volcanology and Geothermal Research* 132(2–3), pages 241–251. DOI: 10.1016/s0377-0273(03)00348-2.

Rader, E., L. Vanderkluysen, and A. Clarke (2017). "The role of unsteady effusion rates on inflation in long-lived lava flow fields". *Earth and Planetary Science Letters* 477, pages 73–83. DOI: 10.1016/j.epsl.2017.08.016.

Sehlke, A., A. Whittington, B. Robert, A. Harris, L. Gurioli, and E. Médard (2014). "Pahoehoe toaa transition of Hawaiian lavas: an experimental study". *Bulletin of Volcanology* 76, pages 1–20. DOI: 10.1007/s00445-014-0876-9.

Shelly, D. and W. Thelen (2021). "High resolution earthquake catalogs from the 2018 Kīlauea eruption sequence". *U.S. Geological Survey data release*. DOI: 10.5066/P9DMIFMW.

Sparks, R. S. J., H. Pinkerton, and G. Hulme (1976). "Classification and formation of lava levees on Mount Etna, Sicily". *Geology* 4(5), page 269. DOI: 10.1130/0091-7613(1976)4<269:cafoll>2.0.co;2.

Tarquini, S. and M. de'Michieli Vitturi (2014). "Influence of fluctuating supply on the emplacement dynamics of channelized lava flows". *Bulletin of Volcanology* 76, pages 1–13. DOI: 10.1007/s00445-014-0801-2.

Zoeller, M. H., F. A. Trusdell, and R. B. Moore (2019). *Digital database of the geologic map of the middle east rift geothermal subzone, Kīlauea Volcano, Hawai'i*. Technical report. U.S. Geological Survey. DOI: 10.3133/ds1111.